Simulation of multiphase flows using a modified upwind-splitting scheme

David J. Robbins, R. Stewart Cant and Lynn F. Gladden

Abstract—A robust AUSM$^+$ upwind discretisation scheme has been developed to simulate multiphase flow using consistent spatial discretisation schemes and a modified low-Mach number diffusion term. The impact of the selection of an interfacial pressure model has also been investigated. Three representative test cases have been simulated to evaluate the accuracy of the commonly-used stiffened-gas equation of state with respect to the IAPWS-IF97 equation of state for water. The algorithm demonstrates a combination of robustness and accuracy over a range of flow conditions, with the stiffened-gas equation tending to overestimate liquid temperature and density profiles.

Keywords—Multiphase flow, AUSM+ scheme, liquid EOS, low Mach number models

I. Introduction

Simulation of multiphase flows is a well-established field in computational fluid dynamics. Modern commercial solvers [1] employ a range of methods, such as the mixture model [2], volume-of-fluid model [3] or the Euler-Euler two-fluid approach [4]. These solvers are generally pressure-based and assume incompressibility of the liquid phase. For simulation of a multiphase flow in a chemical reactor, the incompressible assumption is unsatisfactory. New density-based algorithms are typically tested using the stiffened-gas equation of state or Tait's equation of state due to their simplicity and ability to solve phenomena such as severely non-isentropic shocks [5]. Commercial codes recommend the use of correlations for determination of liquid properties such as density to avoid inaccuracies associated with the cubic equations of state such as Peng-Robinson or Soave-Redlich-Kwong [6].

For discretisation of the convective fluxes, the AUSM$^+$-upwind scheme has been employed successfully by several authors to simulate multiphase flow in simple test cases [7]–[11]. Difficulties associated with hyperbolicity and stiffness of multiphase models can be remedied by either employing an interfacial pressure term [12] or using preconditioning of the mass matrix [13]. The AUSM$^+$-upwind scheme is known to be excellent at resolving flow discontinuities whilst remaining cheap and not requiring explicit knowledge of the system eigenvalues, and is therefore chosen in this study as the convective flux discretisation scheme [14].

In this paper, we address the trade-off between robustness, resolution and physically meaningful solutions when utilising

D. Robbins (corresponding author) and L. Gladden are with the Department of Chemical Engineering and Biotechnology, University of Cambridge, Pembroke Street, Cambridge CB2 3RA, UK. Email: djr57@cam.ac.uk.

S. Cant is with the Department of Engineering, University of Cambridge, Trumpington Street, Cambridge CB2 1PZ, UK.

different equations of state for water. An algorithm based on the AUSM$^+$ scheme has been formulated which is simple to use and can be extended to incorporate other equations of state. The impact of the discretisation method for the differential source terms is also compared by employing a standard central scheme and one modifed to use the upwind mechanism.

II. Numerical method

This section will introduce the numerical method employed in the code PULSAR, by detailing the field equations, spatial and temporal discretisation methods, source terms, initial and boundary conditions, equations of state and the primitive variable reform procedure.

The algorithm which has been employed is based on a two-fluid model in which the pressure is assumed to be at equilibrium between the two phases, such that $p_l = p_g$ where p_i is the pressure of the ith phase and l and g denote the liquid and gas phases respectively. The set of partial differential equations solved in this study are the one-dimensional inviscid two-fluid effective field modelling equations:

$$\frac{\partial \mathbf{W}_i}{\partial t} + \frac{\partial \mathbf{F}_i}{\partial x} = \mathbf{S}_i^d + \mathbf{S}_i^{nd}, \tag{1}$$

where $\mathbf{W}$ is the vector of conservative variables, $\mathbf{F}$ is the convective flux vector and $\mathbf{S}^d$ and $\mathbf{S}^{nd}$ are the vectors of differential and non-differential source terms respectively. These are defined as:

$$\mathbf{W}_i = \left(\alpha\rho, \alpha\rho u, \alpha\rho E\right)_i^\top \tag{2}$$

$$\mathbf{F}_i = \left(\alpha\rho u, \alpha\rho u^2 + \alpha p, \alpha\rho u H\right)_i^\top \tag{3}$$

$$\mathbf{S}_i^d = \left(0, p\frac{\partial \alpha}{\partial x} + F^{nv}, -p\frac{\partial \alpha}{\partial t} + u^{int}F^{nv}\right)_i^\top \tag{4}$$

$$\mathbf{S}_i^{nd} = \left(0, \alpha\rho g + F^D, \alpha\rho u g + u^{int}F^D\right)_i^\top, \tag{5}$$

where α is the phasic volume fraction, ρ the density, u the velocity in the x-direction, E the total energy, p the pressure, H the total enthalpy, F^{nv} the non-viscous differential source terms (such as interfacial pressure), u^{int} the interphase velocity, g the gravitational acceleration and F^D the interphase drag force.

A. Spatial discretisation

The convective fluxes are discretised using the AUSM$^+$-upwind scheme [14]. For each fluid, firstly we calculate the interface speed of sound a_f and the corresponding left and right Mach number M_L/M_R states:

$$a_f = \sqrt{a_L a_R}, \ M_{L/R} = \frac{u_{L/R}}{a_f}. \qquad (6)$$

The left and right Mach number states are used to calculate the phasic pressure at the interface $(\alpha p)_f$ and the Mach number at the interface, M_f:

$$(\alpha p)_f = \mathcal{P}^+ (M_L) (\alpha p)_L + \mathcal{P}^- (M_R) (\alpha p)_R \qquad (7)$$

$$M_f = \mathcal{M}^+ (M_L) + \mathcal{M}^- (M_R), \qquad (8)$$

where $\mathcal{P}^\pm$ and $\mathcal{M}^\pm$ are polynomial functions defined as

$$\mathcal{P}^\pm (M) = \begin{cases} \mathcal{M}_1^\pm / M & \text{if } |M| \geq 1 \\ \pm \mathcal{M}_2^\pm \left(2 \mp M - 16 A M \mathcal{M}_2^\mp \right) & \text{else;} \end{cases} \qquad (9)$$

$$\mathcal{M}^\pm (M) = \begin{cases} \mathcal{M}_1^\pm & \text{if } |M| \geq 1 \\ \pm \mathcal{M}_2^\pm \left(1 \mp M - 16 B \mathcal{M}_2^\mp \right) & \text{else;} \end{cases} \qquad (10)$$

$$\mathcal{M}_1^\pm (M) = \frac{1}{2} (M \pm |M|) \qquad (11)$$

$$\mathcal{M}_2^\pm (M) = \pm \frac{1}{4} (M \pm 1)^2, \qquad (12)$$

where A and B are constants, defined in this study as $3/16$ and $1/8$ respectively. The phasic mass flux at the interface $\dot{m}_f$ is then calculated by an upwinding scheme based on the direction of the interface Mach number:

$$\dot{m}_f = a_f \left[\frac{\alpha_L \rho_L}{2} (M_f + |M_f|) + \frac{\alpha_R \rho_R}{2} (M_f - |M_f|) \right] \qquad (13)$$

From this, the convective fluxes at the interface can be calculated and allocated to the left and right nodes:

$$\alpha \rho u \phi = \frac{\dot{m}_f}{2} (\phi_L + \phi_R) + \frac{|\dot{m}_f|}{2} (\phi_L - \phi_R), \qquad (14)$$

where $\phi = (1, u, H)^\top$ are the convected variables of mass, momentum and energy.

The low-Mach number model used in this work is a modified version of that presented by Liou et al. [10], which diffuses the interface Mach number and pressure as per

$$M_f = M_f - K_p \max \left(1 - \bar{M}^2, 0 \right) \frac{p_R - p_L}{\bar{\rho} \bar{a}^2} \qquad (15)$$

$$(\alpha p)_f = (\alpha p)_f - K_u \mathcal{P}^+ (M_L) \mathcal{P}^- (M_R) \bar{\rho} \bar{a} (u_R - u_L)(\alpha_R - \alpha_L) \qquad (16)$$

where $\bar{\phi}$ denotes an arithmetic-averaged quantity of the left and right states. Unlike the model of Liou, the speed of sound used is the arithmetic-averaged phasic speed of sound, not the mixture speed of sound. We have also added a volume fraction term in the pressure diffusion. The value of the constants K_p and K_u varies on a test-case basis between 0 (i.e. no low-Mach number diffusion) and 0.5.

B. Temporal discretisation

A simple forward-Euler method is used for temporal discretisation of the system of equations in equation 1 at node m:

$$\mathbf{W}_m^{t+\Delta t} = \mathbf{W}_m - \frac{\Delta t}{\Delta x} \mathbf{R}_m^f + \Delta t \left(\mathbf{R}_m^{s,d} + \mathbf{R}_m^{s,nd} \right), \qquad (17)$$

where t and $t + \Delta t$ is the current and proceeding time levels respectively and $\mathbf{R}_m^\psi$ represents the nodal residual of a quantity ψ, for example $\mathbf{R}_m^f$ is the residual of convective fluxes resulting from the difference in the inflow and outflow at the node m. The global minimum time step Δt is determined from an assumed volume fraction weighted averaged of the single-phase style convective spectral radius:

$$\Delta t = \lambda \min_m \left[\frac{\alpha_l \Delta x}{|u_{l,m}| + a_{l,m}} + \frac{\alpha_g \Delta x}{|u_{g,m}| + a_{g,m}} \right], \qquad (18)$$

where λ is a CFL-type number. This number is generally in the range of 0.1 - 0.5 but is generally problem-dependent; values above 1 are entirely plausible for a test case containing no large flow gradients.

C. Source terms

1) Differential source terms: The interfacial pressure is an important differential source term used to render the system of equations hyperbolic. The interfacial pressure force is defined as

$$F_i^{nv} = (p^{\text{int}} - p) \frac{\partial \alpha_i}{\partial x}. \qquad (19)$$

We have incorporated three different methods for determining the interfacial pressure p^{int}; the model of Stuhmiller [12] and two (denoted 'simple' and 'full') proposed by Liou et al. in [10] The details of these models can be found in the appropriate references. The interfacial velocity is required for the energy differential source term; this is simply defined in this work as

$$u^{\text{int}} = \frac{1}{2} (u_g + u_l) \qquad (20)$$

The differential source terms require discretisation of the $p \, \partial \alpha / \partial x$ term. This has been achieved by either employing a central scheme

$$\left(p \frac{\partial \alpha}{\partial x} \right)_m^t = p_m^t \frac{(\alpha_i)_{m+1}^t - (\alpha_i)_{m-1}^t}{2 \Delta x}, \qquad (21)$$

or by employing the AUSM$^+$-up scheme as per

$$\left(p \frac{\partial \alpha}{\partial x} \right)_m^t = \frac{p_m^t}{\Delta x} \left[\left((\alpha_i)_L \mathcal{P}^+ (M_{i,L}) + (\alpha_i)_R \mathcal{P}^- (M_{i,R}) \right)_{m+\frac{1}{2}}^t \right.$$
$$\left. - \left((\alpha_i)_L \mathcal{P}^+ (M_{i,L}) + (\alpha_i)_R \mathcal{P}^- (M_{i,R}) \right)_{m-\frac{1}{2}}^t \right]. \qquad (22)$$

This allows the differential to be calculated as part of the standard convective flux solver whilst retaining consistent discretisation techniques for the convective fluxes and the

differential source terms. Note that this discretisation is applied *both* to the pressure and the interfacial pressure sources, where p_m in the above equation is replaced by the term $(p^{\text{int}} - p)_m$.

The time differential of the volume fraction required for the energy source is discretised as

$$\left(p\frac{\partial \alpha}{\partial t}\right)_m^t = p_m \frac{(\alpha_i)_m^t - (\alpha_i)_m^{t-1}}{\Delta t^{t-1}}, \qquad (23)$$

where t denotes the current time step and $t - 1$ denotes the previous time step. This requires that the time-step and volume fraction from the previous iteration are stored.

2) Non-differential source terms: The non-differential drag and gravity source terms are treated very simply:

$$(\alpha_i \rho_i g)_m^t = (\alpha_i)_m^t (\rho_i)_m^t g \qquad (24)$$

$$(\alpha_i \rho_i u g)_m^t = (\alpha_i)_m^t (\rho_i)_m^t (u)_m^t g \qquad (25)$$

$$(F_i^D)_m^t = C_f \alpha_m^t \left(1 - \alpha_m^t\right) (\rho_g)_m^t \left((u_g)_m^t - (u_l)_m^t\right), \qquad (26)$$

where C_f is a (positive) drag coefficient for liquid drag calculations, and $F_l^D = -F_g^D$.

D. Equations of state

In this work, we employ one of two liquid equations of state (EOS) to link the thermodynamic quantities of density, speed of sound and internal energy to the pressure and temperature. The first is the stiffened-gas model:

$$\rho_l = \frac{\gamma_l}{\gamma_l - 1} \frac{p + p_0}{C_{p,l} T_l} \qquad (27)$$

$$e_l = \frac{C_{p,l} T_l}{\gamma_l} + \frac{p_0}{\rho_l} \qquad (28)$$

$$a_l = \sqrt{(\gamma_l - 1) C_{p,l} T_l}, \qquad (29)$$

with constants $\gamma_l = 2.8$, $p_0 = 8.5 \times 10^8$ Pa and $C_{p,l} = 4186$ J/kg K for water.

The second equation of state selected is the IAPWS-IF97 water equation of state, formulated in terms of the Gibbs free energy [15]. This equation of state serves as a reference for which to compare the stiffened-gas and correlations due to its high level of accuracy. For example, the maximum deviation in specific volume, enthalpy and speed of sound are $\pm 0.05\%$, ± 0.2 kJ/kg and $\pm 1\%$ respectively. The specific volume v_l, specific internal energy e_l and speed of sound a_l are determined in terms of the derivatives of the Gibbs free energy g as

$$v_l = \left(\frac{\partial g}{\partial p}\right)_T \qquad (30)$$

$$e_l = g - T\left(\frac{\partial g}{\partial T}\right)_p - p\left(\frac{\partial g}{\partial p}\right)_T \qquad (31)$$

$$a_l = v_l \sqrt{-\left(\frac{\partial p}{\partial v}\right)_S} \qquad (32)$$

where the subscripted S implies the differential is calculated at constant entropy. The density is then found by taking the

inverse of the specific volume. The list of constants used and the calculation of the Gibbs free energy can be found in the original paper [15].

The ideal gas law is employed for the gas phase:

$$\rho_g = \frac{p}{R_g T_g} \qquad (33)$$

$$e_g = \frac{R_g T_g}{\gamma_g - 1} \qquad (34)$$

$$a_g = \sqrt{\gamma_g R_g T_g}, \qquad (35)$$

where R_g is the specific gas constant for air and the adiabatic index is defined as $\gamma_g = 1.4$.

E. Primitive variable updating

Upon calculating the conservative variables at the next time step, the velocities, total energies and internal energies can be immediately determined:

$$u_i^{t+\Delta t} = \frac{(\alpha_i \rho_i u_i)^{t+\Delta t}}{(\alpha_i \rho_i)^{t+\Delta t}} \qquad (36)$$

$$E_i^{t+\Delta t} = \frac{(\alpha_i \rho_i E_i)^{t+\Delta t}}{(\alpha_i \rho_i)^{t+\Delta t}} \qquad (37)$$

$$e_i^{t+\Delta t} = E_i^{t+\Delta t} - \frac{\left(u_i^{t+\Delta t}\right)^2}{2} \qquad (38)$$

The equations of state are used to determine the pressure, voidage and density by implicit root-finding. A standard secant method is employed for robustness. The two initial guesses are defined by the current pressure level in the fluid, and the function $F(p, T)$ for which the solution is desired is given by:

$$F(p, T) = 0 = \left[1 - \frac{(\alpha_g \rho_g)^{t+\Delta t}}{\rho_g}\right] \rho_l - (\alpha_l \rho_l)^{t+\Delta t}, \qquad (39)$$

where the $(\alpha_i \rho_i)^{t+\Delta t}$ terms are known values, and the other variables are updated in the secant loop. For the case of the stiffened-gas, the liquid density can be written in terms of $\rho_l = \rho_l(e_l, p)$ by simple substitution:

$$\rho_l = \frac{p + \gamma_l p_0}{(\gamma_l - 1) e_l}, \qquad (40)$$

and thus the stiffened-gas equation gives a closed-loop for updating pressure, with liquid temperature determined immediately after finding the root of the function from the internal energy using the pressure at the proceeding time step. For the IAPWS-IF97 equations of state, $\rho_l = \rho_l(T_l, p)$ and $e_l = e_l(T_l, p)$ cannot be closed explicitly and thus an inner loop is required to determine the temperature at each intermediate pressure step from the internal energy. This is performed with a Newton-Raphson procedure using the explicitly-defined gas temperature as the initial first guess, and usually converges within approximately three to five iterations to a residual of the order 10^{-8}.

Once the pressure, temperatures and densities have been calculated at the new time step, the speed of sound is updated

using the appropriate thermodynamic relations and finally the gas void fraction is given by

$$\alpha_g = \frac{(\alpha_g \rho_g)^{t+\Delta t}}{\rho_g}, \tag{41}$$

which closes the liquid volume fraction using $\alpha_l + \alpha_g = 1$.

F. Boundary conditions and simulations

Boundary conditions are implemented with the ghost-cell method. Inlet cells have all values specified except pressure, which is extrapolated from the next interior cell. Outlet cells extrapolate all values from the closest interior cell except for the pressure, which is specified. All simulations are performed on one of two machines; the first an Intel Xeon E5507 workstation with 12 GB DDR3 RAM running openSUSE Linux 11.1 and the second an AMD X4 955 Black Edition desktop with 8 GB DDR3 RAM running openSUSE Linux 11.4.

III. RESULTS AND DISCUSSION

Three unique test cases have been considered in the testing of the developed algorithm. The first is Ransom's faucet problem [16] which models liquid acceleration under the action of gravity, yielding a sharp discontinuity in the volume fraction profile. This test is evaluated in a transient state (at time $t = 0.5$ s). The vector of primitive variables $\mathbf{P} = (\alpha_g, v_l, v_g, p, T_l, T_g)^\top$ is defined in this problem to be $\mathbf{P} = (0.2, 10.0, 0.0, 10^5, 298, 298)^\top$. Boundary conditions for the inlet and outlet discussed above are set to the initial condition values and the length of the domain is 12 m.

The second test is a moving discontinuity problem, which considers the ability of the algorithm to transmit a shock in volume fraction without disturbing the other fields. The initial condition for this problem is given in left- and right-regions which bisect the domain by $\mathbf{P}_L = (0.9, 10.0, 10.0, 10^5, 300, 300)^\top$ and $\mathbf{P}_R = (0.1, 10.0, 10.0, 10^5, 300, 300)^\top$ respectively. The inlet ghost node is located on the left of the domain and the outlet ghost node is located on the right of the domain, and take their defined values from the initial conditions. The length of the domain is 1 m.

The final test is Toumi's shock-tube problem [17] which tests the ability of the algorithm to resolve pressure shocks of the order of magnitude 10^7 Pa. The initial condition for this case is given by bisecting the domain, with $\mathbf{P}_L = (0.25, 0.0, 0.0, 2 \times 10^7, 308.15, 308.15)^\top$ and $\mathbf{P}_R = (0.10, 0.0, 0.0, 1 \times 10^7, 308.15, 308.15)^\top$ the conditions for the left and right states respectively, which also locate the inlet and outlet ghost nodes. The length of the domain is 10 m.

A. Ransom's faucet problem

This problem features the acceleration of a liquid column under the action of gravity, resulting in a transient state in which a discontinuity in the volume fractions is present. The algorithm must therefore be able to resolve a discontinuity
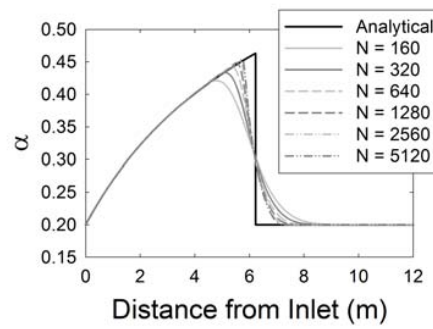
Fig. 1.   Grid study for Ransom's faucet problem - transient gas volume fraction profile.

whilst maintaining stability in the other fluid fields. Analytical solutions for the volume fraction and liquid velocity are available if it is assumed that interphase forces are negligible and the pressure gradient is neglected and are available in the literature [8], [16].

Grid resolutions ranging from 160 nodes to 5120 nodes are tested in in order to show grid convergence and to select an appropriate grid size for subsequent simulations. For the grid independence simulations, the drag source term was neglected and constant values used were $\lambda = 0.5$ and $\sigma = 2.0$. No low-Mach number model was used, and the IAPWS-IF97 equation of state was employed. The results presented in Figure 1 demonstrate the grid convergence for the correlations. With each subsequent level of grid refinement, the resolution of the discontinuity increases as expected. The results correspond well to the analytical solution and oscillations are minimised due to the dampening effect of the interfacial pressure. On the basis of the tradeoff between resolution and computational time, a grid of 1280 nodes was selected for evaluating the EOS and interfacial pressure models.

Figures 2 and 3 shows the impact of the selected interfacial pressure model at resolving the gas volume fraction and the pressure for the correlations. The same constant values and correlations as per the grid size simulations were employed. For the volume fraction profile, it is immediately evident that the interfacial pressure term serves to eliminate the unphysical
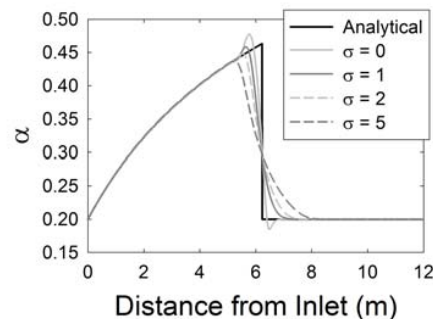
Fig. 2.   Impact of interfacial pressure on resolution of gas volume fraction discontinuity - Stuhmiller models with constant values $\sigma = 0$ to 5 in Ransom's faucet problem.
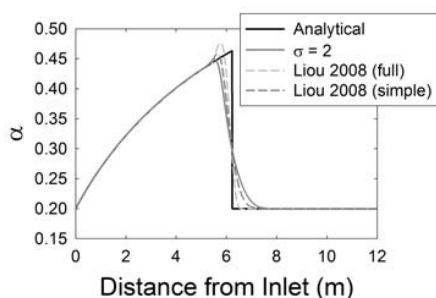
Fig. 3. Impact of interfacial pressure on resolution of gas volume fraction discontinuity - Liou et al. (2008) models and the Stuhmiller model with $\sigma = 2$ in Ransom's faucet problem.

oscillations present in front and behind of the discontinuity. The simple model of Liou eliminates the post-shock oscillation but not the oscillation in front of the shock, whilst the full model, designed to employ interfacial pressure but not over-dissipate, shows a slightly greater amplitude of oscillation than the Stuhmiller model of $\sigma = 2$. Increasing the value of the σ constant yields a solution more bound by the analytical solution, but diffuses the discontinuity. For the pressure profile, the choice of interfacial pressure model has a large impact. Selection of no model or the simple model creates a large departure from from the pressure profiles generated by the Stuhmiller model or the full Liou model. Over-diffusion with $\sigma = 5$ generates an unphysical pressure drop in the domain. The departure from the discontinuity is also evident in the gas velocity profiles, but the departure is not as severe as in the pressure case. The over-diffused case simply smears the discontinuity of gas pressure, whilst using no interfacial pressure model or the simple model generate unphysical oscillations before and after the shock. The Stuhmiller model using a constant value of $\sigma = 2$ is thus a good starting benchmark for investigating the impact of the interfacial pressure term on a per-problem basis.

Finally, the impact of the discretisation of the source terms was investigated by employing either a central scheme or the AUSM$^+$-up scheme to discretise the differential volume fraction sources. In this problem, employing a central scheme with a modest amount of interfacial pressure ($\sigma = 2$), a
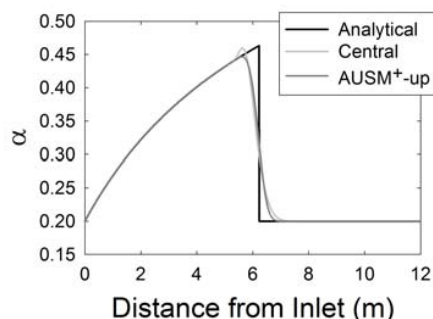
small overshoot is still observed prior to the discontinuity in the central scheme. As can be seen in Figure 4, employing the AUSM$^+$-up term for discretisation of both the pressure and interfacial pressure sources eliminates this oscillation and facilitates a smooth and sharp resolution of the discontinuity. It was noted (not shown here) that employing the AUSM$^+$-up scheme for only the $p \cdot \partial \alpha / \partial x$ term - not for the interfacial pressure term - yields a similar oscillation as the central scheme but of smaller amplitude prior to the discontinuity due to the inconsistency in discretisation techniques of the pressure terms. The consistent discretisation outlined in the methodology eliminates this oscillation prior to the resolved discontinuity.

B. Moving discontinuity problem

The moving discontinuity problem tests that the code can maintain a high resolution of the interface whilst retaining smooth and undisturbed profiles of the other fields fields, particularly the pressure field, also known as the so-called pressure non-disturbing criterion [18]. Grid dependence was tested by simulating a range of resolutions from 100 to 5000 nodes. These simulations used the Stuhmiller model with $\sigma = 2$, no low-Mach number model and a temporal constant of $\lambda = 0.3$. No gravity or drag sources are used in this problem and the IAPWS-IF97 equation of state was employed. Figure 5 shows that the AUSM$^+$-up again demonstrates excellent resolution of the discontinuity even at coarse grids, with progressively better resolution as the grid is refined. A grid resolution of 1000 nodes was selected based on the trade-off between computational expense and accuracy for further simulations.

Figure 6 compares the solutions for the pressure and liquid velocity profiles using the central and AUSM$^+$ discretisation schemes of the void fraction source terms. The pressure profile shows significant disturbance when the central scheme is employed, with the non-disturbance criterion fulfilled for the AUSM$^+$-up scheme. The liquid velocity shows a large departure from equilibrium at the point of the discontinuity in the domain for the central scheme, confirming that the central scheme returns unphysical results for points of discontinuities. These could potentially be reduced by employing methods such as artificial viscosity and residual smoothing, but given that the AUSM$^+$-up scheme is already employed for the
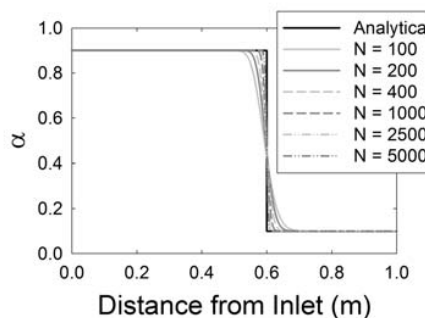

Fig. 4. Impact of source term discretisation method pressure on resolution of gas volume fraction discontinuity in Ransom's faucet problem.

Fig. 5. Grid refinement study for the moving discontinuity test case.
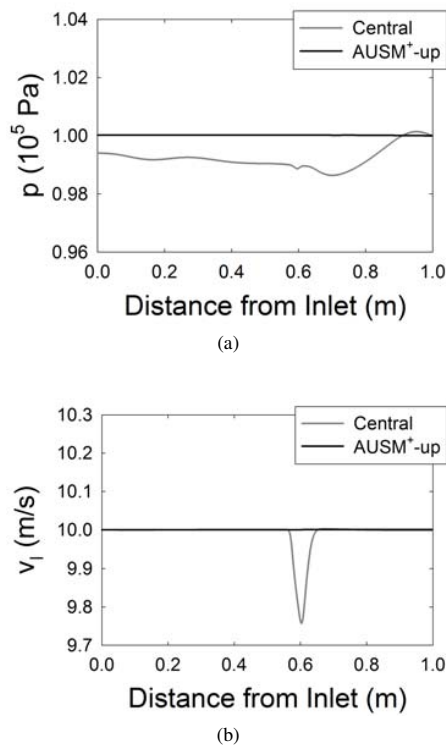
(a)

(b)

Fig. 6. Impact of the source term discretisation method on the (a) pressure and (b) liquid velocity profiles for the moving discontinuity problem.

convective fluxes (and thus no extra calculations are required to determine the differential of volume fraction) it seems pertinent to select this discretisation scheme.

C. Toumi's shock tube

This test case was selected due to its widespread use as a test case for multiphase flow, to test robustness of the code under more challenging conditions and to evaluate the accuracy of the stiffened-gas equation of state compared to the IAPWS-IF97 equation of state. For this test case, grids ranging from 200 to 10 000 nodes were tested in order to determine the optimal grid size. In the grid size simulations, other parameters used were $\lambda = 0.1$, $\sigma = 2.0$ and the modified low-Ma model was enabled due to the sharp pressure
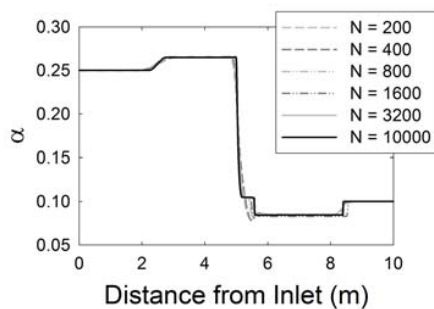

Fig. 7. Grid refinement study for Toumi's shock tube test case.

gradients in the flow. Gravity and drag forces were again disabled. The grid dependency test in Figure 7 shows a greater difference between the more highly-resolved grids than the previous test cases, with the finest grid resolving five distinct volume fraction surfaces and the coarser grids generating more smoothed profiles with fewer surfaces. A grid of 3200 nodes was selected due to its similarity in resolution to the 10 000 node solution.

Figure 8 shows the simulated profiles of gas volume fraction, liquid velocity, liquid temperature and liquid mass flux for Toumi's shock tube test problem. The voidage profiles for both equations of state present excellent agreement, with slight deviations noted between the first two surfaces. The liquid velocity profile for the stiffened-gas equation diverges from the profile predicted by the IAPWS-IF97 equation of state, with consistent under-prediction of the liquid velocity. This is due to the inaccurate prediction of density and speed of sound by the stiffened-gas equation of state impacting the calculation of mass flux at the cell faces. The liquid temperature profile is of higher amplitude for the stiffened-gas than the IAPWS-IF97 equation of state, which predicts that the range of liquid temperatures in the domain should be smaller. Whilst the range of temperatures inside the domain are very different, the overall shape of the profile predicted by the stiffened-gas equation of state is correct. Use of a stiffened-gas equation of state is therefore only advisable as a cheap method to test a code rather than to simulate a possible solution for a problem. The liquid mass flux profile for the stiffened-gas profile however matches the IAPWS-IF97 profile remarkably well, due to the countering effects of the under-predicted liquid velocity and over-predicted density. This is supported by considering the water density in the high-pressure domain by substitution of the appropriate values into the stiffened-gas density equation, with approximately 5%, over-prediction of water density compared to the IAPWS-IF97 equations. The liquid velocities are under-estimated by approximately the same magnitude of relative error, explaining the matching liquid mass flux profiles. This phenomenon is expecially prevalent in this test case given that the difference between p and p_0 is of a lower order of magnitude in a domain of high pressure than a domain of atmospheric pressure, and thus the liquid density equation is more amenable to pressure and temperature changes in the domain.

IV. CONCLUSION

The accuracy of the stiffened-gas equation of state has been compared to the industrial standard IAPWS-IF97 equation of state for water by employing a modified AUSM$^+$-up scheme. The stiffened-gas equation of state was shown to give inaccurate simulations of the flow profiles in comparison to the IAPWS-IF97 equations of state. The modified AUSM$^+$-up scheme was found to give excellent resolution of discontinuities and is robust when coupled to the correct interfacial pressure and low-Mach number models, particularly when used to also discretise differential source terms. It also serves to mitigate against unphysical oscillations around discontinuities. Future work will add real-fluid equations of
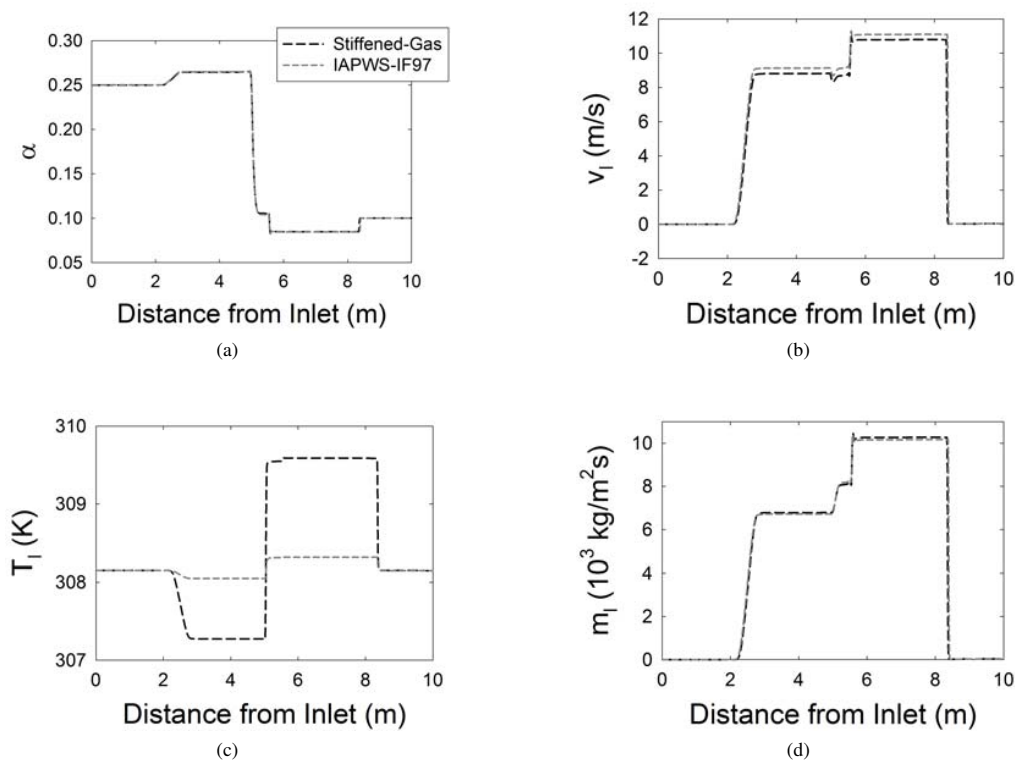
Fig. 8. Profiles of (a) gas volume fraction, (b) liquid velocity, (c) liquid temperature and (d) liquid mass flux for the stiffened-gas and IAPWS-IF97 equations of state for Toumi's shock tube test case.

state such as Peng-Robinson in order to simulate arbitrary liquids, and the one-dimensional algorithm will be extended to higher dimensions.

REFERENCES

[1] *FLUENT Documentation for ANSYS 13*, ANSYS, Inc.
[2] S. Soo, "On one-dimensional motion of a single component in two-phases," *International Journal of Multiphase Flow*, vol. 3, pp. 79–82, 1976.
[3] C. Hirt and B. Nichols, "Volume of Fluid (VOF) method for the dynamics of free boundaries," *Journal of Computational Physics*, vol. 39, pp. 201–225, 1975.
[4] M. Ishii, *Thermofluid dynamic theory of two-phase flow*. Paris, France: Eyrolles, 1975.
[5] K. Shyue, "A fluid-mixture type algorithm for barotropic two-fluid flow problems," *Journal of Computational Physics*, vol. 200, pp. 718–748, 2004.
[6] *CFX solver theory guide for ANSYS 13*, ANSYS, Inc.
[7] C. Chang and M. Liou, "A new approach to the simulation of compressible multifluid flows with the ausm$^+$ scheme," in *16th AIAA Computational Fluid Dynamics conference*, Orlando, Florida, USA, June 2003.
[8] H. Paillère, C. Corre, and J. García Cascales, "On the extension of the AUSM+ scheme to compressible two-fluid models," *Computers & Fluids*, vol. 32, pp. 891–916, 2003.
[9] C. Chang and M. Liou, "A robust and accurate approach to computing compressible multiphase flow: stratified flow model and AUSM$^+$-up scheme," *Journal of Computational Physics*, vol. 225, pp. 840–873, 2007.
[10] M. Liou, C. Chang, L. Nguyen, and T. Theofanous, "A robust and accurate approach to computing compressible multiphase flow: stratified flow model and AUSM$^+$-up scheme," *AIAA Journal*, vol. 46, pp. 2345–2356, 2008.
[11] Y. Niu, Y. Lin, and C. Chang, "A further work on multi-phase two-fluid approach for compressible multi-phase flows," *Numerical Methods in Fluids*, vol. 58, pp. 879–896, 2008.
[12] J. Stuhmiller, "The influence of interfacial pressure forces on the character of two=phase flow model equations," *International Journal of Multiphase Flow*, vol. 3, pp. 551–560, 1977.
[13] A. Zanotti, C. Méndez, N. Nigro, and M. Storti, "A preconditioning mass matrix to avoid the ill-poised two-fluid model," *Transactions of the ASME*, vol. 74, pp. 732–739, 2007.
[14] M. Liou, "A sequel to AUSM, part II: AUSM$^+$-up for all speeds," *Journal of Computational Physics*, vol. 214, pp. 137–170, 2005.
[15] W. Wagner, J. Cooper, A. Dittmann, K. Kijima, H. Kretzschmar, A. Kruse, R. Mareš, K. Oguchi, H. Sato, I. Stöcker, O. Šifner, Y. Takaishi, I. Tanishita, J. Trübenbach, and T. Willkommen, "The IAPWS industrial formulation 1997 for the thermodynamic properties of water and steam," *Transactions of the ASME*, vol. 122, pp. 150–182, 2000.
[16] V. Ransom, "Numerical benchmark tests," in *Multiphase science and technology*, G. Hewitt, J. Delhaye, and N. Zuber, Eds. Hemisphere publishing coporation, 1987, vol. 3.
[17] I. Toumi, "An upwind numerical method for two-fluid two-phase models," *Nuclear Science & Engineering*, vol. 123, pp. 147–168, 1996.
[18] R. Saurel and R. Abgrall, "A multiphase Godunov method for compressible multifuid and multiphase flows," *Journal of Computational Physics*, vol. 150, pp. 425–467, 1999.